Nanoscale microstructure and chemistry of transparent gahnite glass-ceramics revealed by atom probe tomography

Alexandra L. Mitchell[a,*], Daniel E. Perea[b], Mark G. Wirth[b], Joseph V. Ryan[c], Randall E. Youngman[a], Aram Rezikyan[a], Albert J. Fahey[a], Daniel K. Schreiber[c]

[a] *Corning Research and Development Corporation, 1 Science Center Drive, Painted Post, NY 14870, United States*
[b] *Environmental and Molecular Sciences Laboratory, Earth and Biological Sciences Directorate, Pacific Northwest National Laboratory, P.O. Box 999, Richland, WA 99352, United States*
[c] *Energy and Environment Directorate, Pacific Northwest National Laboratory, P.O. Box 999, Richland, WA 99352, United States*

ARTICLE INFO

Keywords:
Nanocrystalline materials
Atom probe tomography
Nucleation
Microstructure
Glass

ABSTRACT

The nanoscale microstructure and chemistry of a transparent gahnite glass-ceramic and its precursor glass were investigated using atom probe tomography, transmission electron microscopy, and nuclear magnetic resonance spectroscopy. In the annealed precursor glass, statistically significant ZrO clustering was observed along with Si depletion within 2 nm of the ZrO clusters. This clustering is expected to be the first step in the nucleation and crystallization of the nucleating agent, ZrO_2. In the glass-ceramic, gahnite ($ZnAl_2O_4$) crystallites were found to exist in proximal locations to ZrO_2 and not in a core-shell arrangement. The residual glass composition was directly measured by atom probe, showing higher concentrations of Al, Zn, and Zr than previously expected. At the interfaces between the crystallites and residual glass, no enrichment or depletion zones were found. These findings provide answers to outstanding questions surrounding the nucleation and elemental partitioning, microstructure, and the residual glass composition of transparent gahnite glass-ceramics.

Glass-ceramics are partially or entirely crystalline, solid materials formed from a glassy precursor [1]. A controlled heat treatment induces nucleation and growth of the crystalline phase(s). The glass precursor is a non-equilibrium material, and the subsequent crystallization process is also a non-equilibrium, dynamic process. There is often significant uncertainty in the composition and structure of the crystalline products and residual glass, their respective temporal evolution, and specific temperature thresholds required to achieve different outcomes from a given precursor glass composition. Therefore, for each precursor glass composition, it is necessary to experimentally and analytically determine these factors to fabricate glass-ceramic materials that have the desired properties for a given application. Efforts to model and predict glass-ceramic microstructures and properties from first principles and by machine learning techniques have increased in recent years [2-4]. However, significant empirical prior knowledge is required, and more traditional experimental and analytical approaches continue to prevail in guiding material design and in generating understanding.

The spinel glass-ceramic system can produce optically transparent materials. Because of their optical, thermal, and mechanical properties, spinel glass-ceramics have been studied since the late 1960s for applications ranging from substrates for thin films of polycrystalline silicon to transparent armor or protective cover glass for electronic devices [5-12]. For compositions similar to those discussed here, many first order questions have already been answered [11]. For example, ZrO_2 has been identified as the nucleating agent [11]. Gahnite ($ZnAl_2O_4$, the Zn endmember spinel mineral) is the main crystalline phase that crystallizes after ZrO_2 via a heterogeneous nucleation process. The microstructure is uniformly nanocrystalline, and the material's optical transparency is dependent on the size and the arrangement of the crystallites, which can be controlled by changes in precursor glass composition and heat treatment [11]. Finally, many optical, thermal, and mechanical material properties have been characterized and reported for compositions similar to those discussed here [10, 11].

Several questions persist about these otherwise well-studied spinel glass-ceramics, which are addressed here using atom probe tomography (APT) in conjunction with scanning transmission electron microscopy (S/TEM) and nuclear magnetic resonance (NMR) spectroscopy. The application of APT to glass science is still relatively new [13-16]. The key strengths of APT are nominally equal

* Corresponding author.
E-mail address: aandrewsmitchell@gmail.com (A.L. Mitchell).

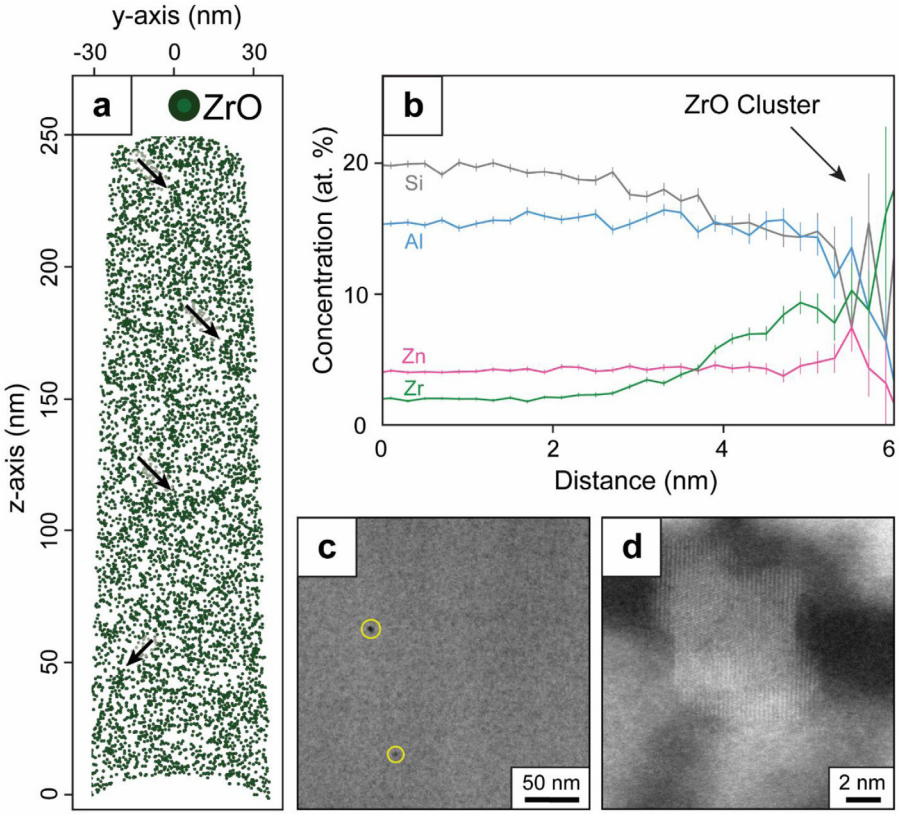

Fig. 1. *High resolution characterization of the annealed precursor glass by APT and S/TEM.* ***a)*** *APT atom-map visualization of ZrO clustering (10 nm image depth) and* ***b)*** *APT proxigram based on a ZrO isosurface of 4.5 at.% showing Si depletion, constant Al and Zn, and Zr enrichment.* ***c)*** *BF-S/TEM image exhibiting mottled contrast consistent with ZrO clustering and scattered ZrO_2 crystals (3–10 nm, yellow circles),* ***d)*** *High-resolution HAADF S/TEM image of a circled, dark contrast region showing crystalline structure consistent with ZrO_2. Note: the color contrast is inverted between the BF-S/TEM image in c) and the HAADF S/TEM image in d). APT and S/TEM data were measured on different liftouts from the same annealed glass sample.*

sensitivity to all elements in the periodic table, sub-nm spatial resolution, and 3D compositional reconstructions of the analyzed volume [17, 18]. APT does not, however, natively identify crystal structure or phase and has a relatively small field of view (~100 × 100 × 100 nm^3) compared to S/TEM samples (~micrometers in lateral area). APT is, however, uniquely suited to address outstanding questions about this gahnite glass-ceramic system that were previously difficult or impossible to address including: 1) Do elements partition or cluster prior to heat treatment?; 2) What is the spatial arrangement of the main crystalline phase (gahnite) relative to the ZrO_2 nucleating agent?; 3) What is the composition of the residual glass, and does it exhibit local depletion or enrichment of species near the residual glass/crystal interfaces? In the work presented here, APT is used in combination with S/TEM and NMR to address these open questions relating to the nucleation, composition, and microstructure in the spinel glass-ceramic system. Details of the instruments used and analysis parameters are provided in the supplemental materials along with information about precursor glass fabrication and the heat treatment method used to form the glass-ceramic.

Crystallite nucleation in glass-ceramics is exceptionally difficult to study. In the spinel glass-ceramic system, it is still a matter of debate whether crystallization of the main spinel phase results from phase separation within the precursor glass [12] or due to the initial crystallization of nucleating agents such as ZrO_2 [5, 11]. In Fig. 1a and SM Video 1, the APT data capture a snapshot in time of the nucleation process after the precursor glass was melted, quenched, then annealed at 600°C. Statistically significant clustering of ZrO was observed within an otherwise homogeneous glass. Frequency distribution analysis was conducted on a centrally located 30 × 30 × 200 nm^3 cube region of interest (ROI) where the rejection of the null hypothesis (p-value < 0.01) indicated that the atoms in the sample were not randomly distributed [19]. For ZrO, clustering was observed as indicated by a p-value of <0.0001, using a 200-ion bin size and excluding unranged ions (SM Fig. 4 and SM Table 1). All other ions had p-values ≥ 0.03, indicating a random distribution in the annealed precursor glass. Upon closer examination of the interface between the ZrO clusters and the surrounding glass using a proximity histogram (i.e. proxigram, Fig. 1b [20]), constant values of Zn and Al and depletion of Si were evident in the 2 nm adjacent to the Zr clusters. This observation could suggest that Si is notably incompatible with the Zr cluster, that Zn and Al have a greater affinity for the Zr cluster, or a combination of both hypotheses. The relative enrichment of Al and Zn very close

Table 1
Precursor glass composition (mol%) by inductively coupled plasma optical emission spectroscopy (ICP-OES) and APT. Residual glass composition (mol%) estimated using ^{27}Al MAS NMR compared to measured residual glass composition using APT.

	Precursor Glass		Residual Glass	
Component	ICP	APT	NMR	APT
SiO_2	54.4	55.1	89.5	88.0
Al_2O_3	21.1	22.3	5.8	7.0
ZnO	15.5	15.2	†	2.0
Na_2O	3.8	2.0	4.7	1.8
ZrO_2	5.2	5.5	†	1.1

† Assumed to be 0.

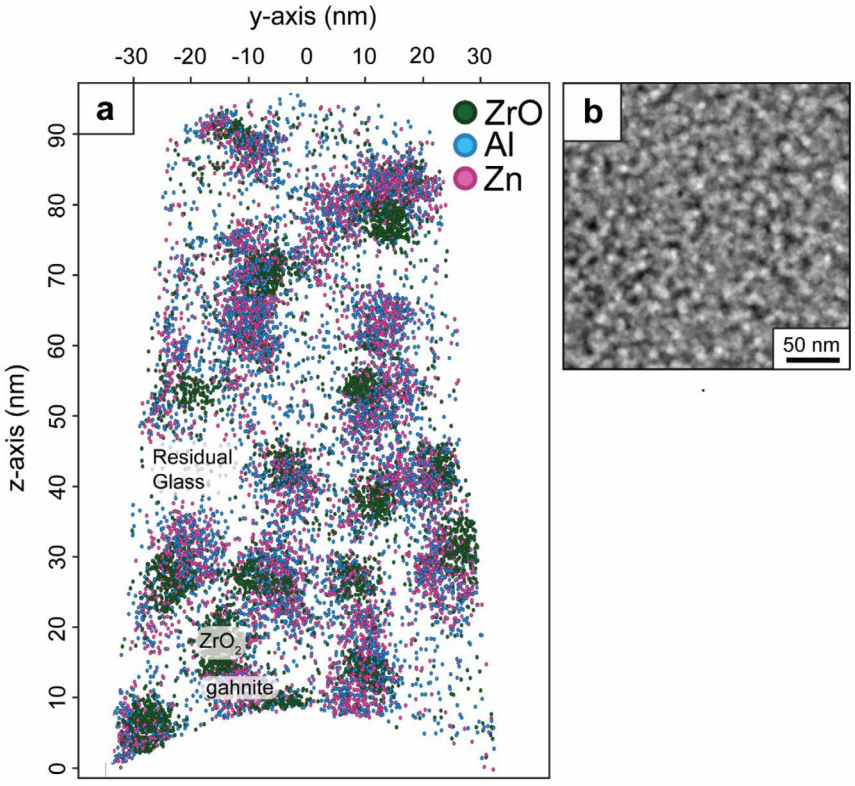

Fig. 2. *Microstructure of gahnite glass-ceramics after heat treatment as visualized via **a)** APT elemental atom-map of the ZrO, Al, and Zn distribution (10 nm image depth) and **b)** HAADF S/TEM where gahnite is medium grey, ZrO_2 is the brightest grey, and residual glass is the darkest areas. Note that the empty space in the APT reconstruction coincides with the residual glass.*

to the Zr clusters could promote heterogenous nucleation of the gahnite phase.

In the bright-field S/TEM (BF-S/TEM) image of the annealed precursor glass (Fig. 1c), mottling is observed throughout the sample. This contrast suggests inhomogeneity on the scale of a few nanometers, in good agreement the ZrO clustering observed by APT. Sparse ZrO_2 crystallites, distinct from the general mottling, were observered in BF-S/TEM and were not observed in the APT data. These crystallites are evident in Fig. 1c as the circled dark spots in the image. They ranged from ~3 nm to ~10 nm in diameter (Fig. 1d). The crystallites are so sparsely distributed that it is likely that the APT specimens did not intersect similar crystallites as the features observed in the APT data were ~ < 1 nm (Fig 1b) compared to the much larger features observed in the TEM data (~3-10 nm) . The complementary APT and BF-S/TEM data suggest that the annealed precursor glass is contemporaneous with the onset of nucleation in some regions (clustering/mottling across the material) and is immediately following the onset of nucleation in other regions (sparse crystallites at the 3–10 nm scale).

The observation of ZrO clustering and sparse ZrO_2 crystallites is consistent with high temperature X-ray diffraction measurements of a compositionally similar glass-ceramic that showed sequential crystallization of ZrO_2 followed by gahnite [11]. The APT data complement these studies by establishing that ZrO first forms localized clusters. It is suspected that these ZrO clusters eventually form critical nuclei for ZrO_2 crystallites, as is apparent in the TEM data. Zr clustering was also observed in extended X-ray absorption fine structure data for Zr-containing Zn, Mg, Ca, and Li aluminosilicates [21]. Heavy element clustering (i.e. Zr) was also found using S/TEM in high angle annular dark field imaging mode (S/TEM-HAADF) in a similar glass composition in the absence of visible crystalline phases [22, 23]. In both the APT data shown in Fig. 1 and the S/TEM-HAADF data in [23], the spatial distribution of the clustering appears to be random, and the residual glass is not yet significantly depleted of Zr.

After heat treatment at 950°C, the precursor glass becomes a three-phase glass-ceramic material consisting of crystalline ZrO_2, crystalline gahnite ($ZnAl_2O_4$), and residual glass (Fig. 2). With 2D imaging techniques, it was not possible to determine if the nucleating agent (crystalline ZrO_2) was in a core-shell relationship with the main crystalline phase (gahnite) or if the crystalline phases were located proximal to one another. In Fig. 2a, Fig. 3, and SM Video 3, the APT data unambiguously show that the ZrO_2 and gahnite are proximal. The ZrO_2 crystals are isolated across the material whereas the gahnite crystals are interconnected (SM Video 2). The 3D, connected morphology of the gahnite is interesting in the context of the material's transparency. It was previously found that if these glass-ceramics were insufficiently nucleated, the gahnite crystallites would grow in a spherulitic pattern [11]. While individual gahnite crystallites remained small (~15 nm), the overall diameters of the spherulitic structures were large enough to interact with the wavelengths of visible light (hundreds of nms), causing scattering and resulting in opaque materials. In the glass-ceramic investigated here, the interconnected but randomly oriented gahnite nanocrystals retain the optical characteristics of the nanoparticles, and the material remains transparent.

As elements partition into the crystalline phases (Zr, Zn, and Al), the composition of the residual glass becomes Na- and Si-rich, and Zr-, Zn-, and Al-poor. In Fig. 4, proxigrams [20] depict composition changes of the primary elements between a) the gahnite crystallites and the surrounding material (a combination of residual glass and ZrO_2 crystallites), b) the ZrO_2 crystallites and the surrounding material (a combination of residual glass and gahnite crystallites), and c) and d) the residual glass and the surrounding phases (a

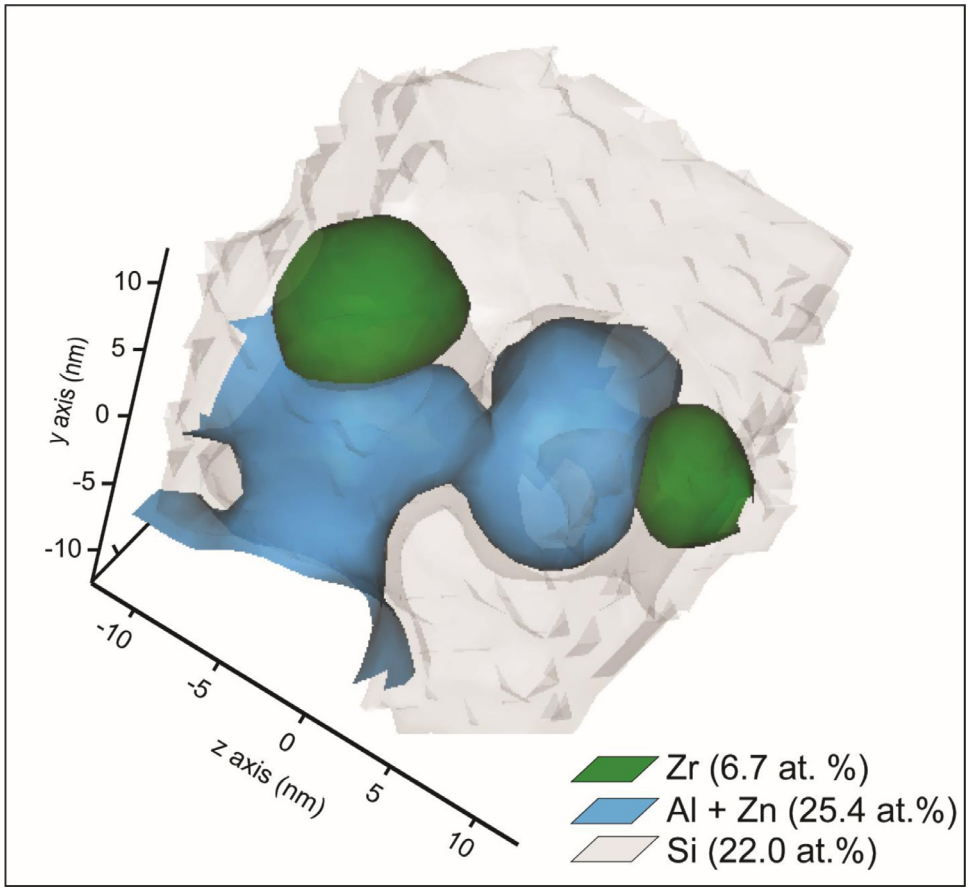

Fig. 3. 25 × 25 × 25 nm^3 subvolume of 3D APT data from the glass-ceramic showing the location of the ZrO_2 nucleating agent proximal to the main crystalline phase (gahnite, $ZnAl_2O_4$). Zr isosurface at 6.7 at.% (green), Al+Zn isosurface at 25.4 at.% (blue), and Si isosurface at 22 at.% (grey). Si isosurface shows the surrounding residual glass.

combination of ZrO_2 and gahnite crystallites). The proxigrams were based on isoconcentration surfaces of 4.0 at.% Zr, 17.6 at.% Al + Zn, and 22.0 at.% Si for the ZrO_2, gahnite, and residual glass phases, respectively. Further analysis parameters and O profiles (SM Fig. 5) are included in the supplementary material. Note that each proxigram reports compositions for a single isolated phase (to the right of the dashed lines), whereas the data to the left of the dashed lines report a mixed composition signal from the other two phases.

In the gahnite crystallites (Fig. 4a and SM Fig. 6a), Al and Zn are enriched (~26.2 at.% and ~15.7 at.%) relative to the surrounding material (~5.8 at.% and ~1.1 at.%). Si, Na, and O (~4.4, ~0.6, and ~52.2 at.%, respectively) are depleted relative to the surrounding residual glass and ZrO_2 crystallites (~31.5, ~1.4, and ~58.9 at.%, respectively). Composition profiles from the gahnite into the surrounding material are smooth gradients over a 3-5 nm distance. These gradients (along with the lack of a compositional plateau in the gahnite) suggest that the accuracy of the composition is limited by APT spatial resolution (i.e. there is an artificial mixing of the gahnite and surrounding material over the 3-5 nm gradient). There is no evidence for localized Zn or Al depletion nor Si enrichment adjacent to the gahnite crystallites. In the ZrO_2 crystallites (Fig. 4b and SM Fig. 6b), Zr and O are enriched relative to the surrounding residual glass plus gahnite material (~24.0 at.% and ~64 at.% versus ~1.3 at.% and ~57.0 at.%, respectively). Si, Al, Zn, and Na are depleted relative to the surrounding residual glass plus gahnite material (~6.2, ~3.9, ~1.9, and ~0.7 at.% versus ~22.4, ~13.3, ~5.2, and ~1.2 at.%, respectively). The observed compositions and elemental partitioning are consistent with expectations for both crystalline phases.

In the residual glass (Fig.s 4c and 4d), Si and Na are enriched relative to the crystalline phases (~33.3 at.% and ~1.3 at.% versus <6 at.% and <0.7 at.%, respectively), while Al, Zn, and Zr are depleted to ~5.3, ~0.8, and ~0.4 at.%, respectively, compared to ~23.6, ~12.4, and ~2.7 at.% in the surrounding crystallites. While Al is depleted in the residual glass compared to the precursor glass, it is not entirely consumed by gahnite precipitation and is still present in the residual glass at ~5.3 at.% compared to ~14.7 at.% in the precursor glass.

Significantly, the measured Na concentration in the residual glass (~1.3 at.% or ~1.8 mol%) was lower than expected (~3.0 at.% or ~4.7 mol%). Initially, it was assumed that all Na would partition into the residual glass, but the APT and ^{23}Na magic-angle spinning (MAS) NMR results show that some of the Na partitioned into the gahnite crystals (SM Fig. 6). In the NMR data, a change in the chemical shift of ^{23}Na indicated a change in glass composition after gahnite crystallization (i.e. Si enrichment; Al depletion), which changed the role of Na^+ in the residual glass to more of a network modifier (i.e. non-bridging oxygen [NBO] formation). A non-zero Al fraction in the residual glass would also need to be charge-balanced by modifiers like Na^+. The fitting shown in SM Fig. 6 is consistent with 25% of the Na being in a crystalline environment and 75% of the Na remaining in the residual glass.

In this study, APT also measured a lower overall Na composition in the precursor glass than reported by ICP-OES (Table 1). We partially attribute this discrepancy to an APT quantification error, as it is commonplace for APT to under-report true concentrations of easily-evaporated and mobile alkali species [24, 25]. If migration were present during these analyses, the phenomemon was non-

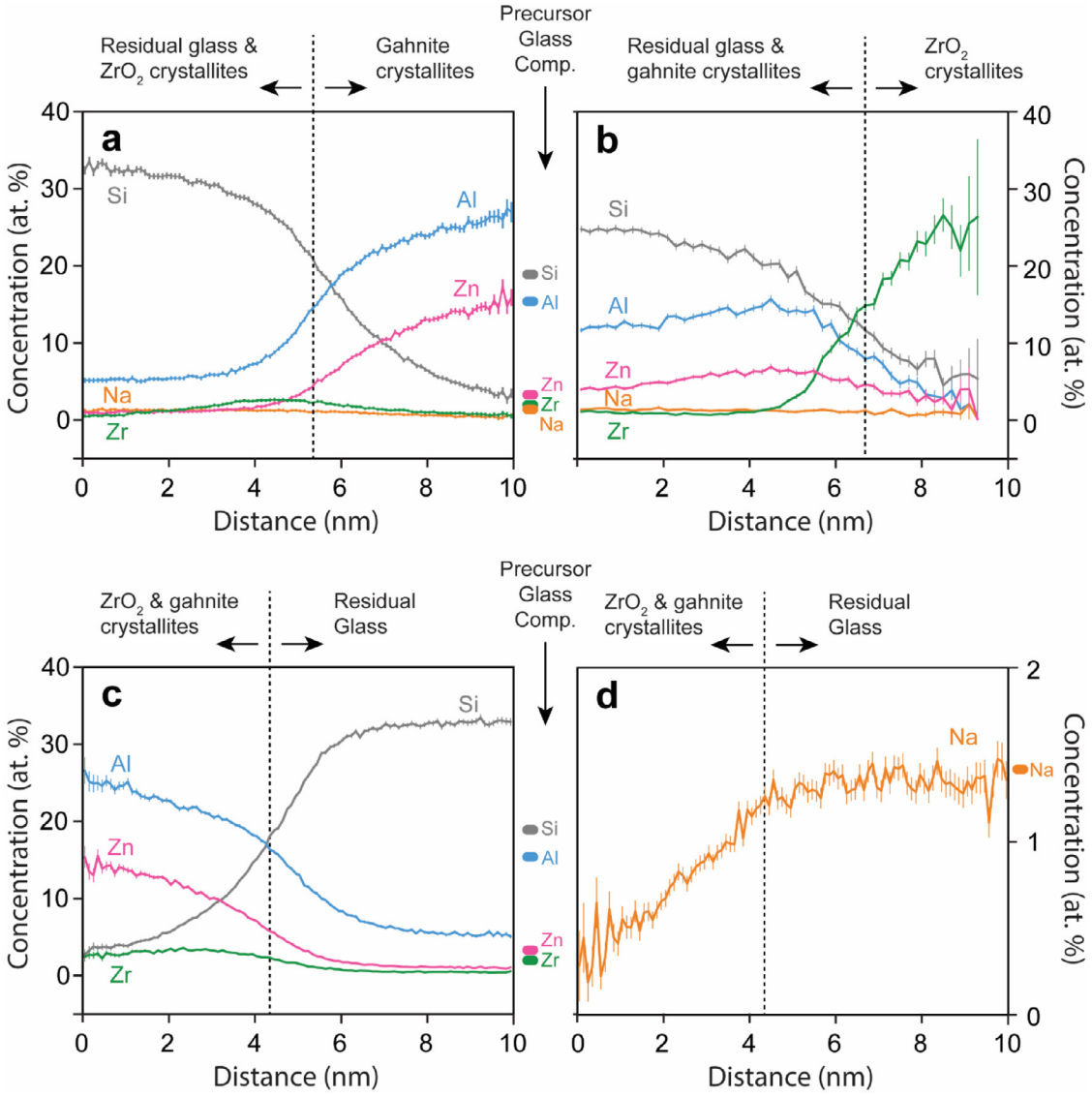

Fig. 4. *APT proxigrams showing the composition profiles for the glass-ceramic between surrounding material (left of dashed line) and isolated* ***a)*** *gahnite crystallites (17.6 at.% Al + Zn isoconcentration surface),* ***b)*** *ZrO_2 crystallites (4.0 at.% Zr isoconcentration surface), and* ***c, d)*** *the residual glass (22 at.% Si isoconcentration surface). The nominal APT-measured precursor glass composition is depicted in the center for comparison for panels a, b, and c and to the right for panel d.*

directional as the measured precursor and residual glass compositions were uniform across the APT specimens.

Table 1 compares the residual glass composition measured directly by APT with an estimate indirectly derived from ^{27}Al MAS NMR data, as described in [11]. The ^{27}Al MAS NMR method assumed that all Zr and Zn were consumed in the crystallization of ZrO_2 and gahnite, respectively, leaving neither of these components in the residual glass. The Al content of the residual glass was then calculated using fits to the NMR data, which determined the amount of tetrahedral (Al^{IV}) and octahedral (Al^{VI}) in the gahnite phase as well as the amount of Al remaining in the residual glass. In this case, 17 at.% Al remained in the residual glass, with 2 at.% Al^{IV} and 81 at.% Al^{VI} partitioned to the gahnite, which was consistent with prior work on gahnite that showed only a small amount of Al^{3+} in the tetrahedral site regardless of heat treatment temperature [26]. Finally, ^{29}Si MAS NMR showed that all SiO_2 partitioned into the residual glass (SM Fig. 7). Given the assumptions built into the NMR-based residual glass estimate, the final values are notably close to those measured by APT. The most significant difference is that the direct measurement via APT revealed small amounts of Zr and Zn remaining in the residual glass after heat treatment that were assumed to be negligible in the calculated NMR composition. This is important because knowledge of the residual glass composition enables the tailored design of the precursor glass composition for optimizing diffusivity during chemical strengthening, refractive index matching between the phases for transparency, viscosity for forming, and chemical durability of the glass-ceramic.

Three open questions about the transparent gahnite glass-ceramic system were addressed using APT data in conjunction with S/TEM and NMR. After annealing, but prior to heat treatment, statistically significant ZrO clustering was observed in the precursor glass with constant Zn and Al and Si depletion in the 2 nm closest to the edge of the ZrO clusters. These observations provide a snapshot into the nucleation process for these glass-ceramics. The residual glass within the glass-ceramic materials was directly measured for the first time, showing evidence for small but significant concentrations of Al, Zn, and Zr in the residual glass. While it was expected that Al would remain in the residual glass, the presence and amount of the Zn and Zr were previously unknown. The 3D morphology of the crystalline phases was also determined; the

glass-ceramic was comprised of isolated ZrO_2 crystallites and interconnected gahnite nanocrystals where the two crystalline phases were located proximal to one another.

Declaration of Competing Interest

The authors declare that they have no known competing financial interests or personal relationships that could have appeared to influence the work reported in this paper.

Acknowledgments

The authors thank the Engineering and Materials Processing department at Corning for batching, melting, and annealing the precursor glass, and Dr. Charlene Smith for helpful discussion. This work was supported by Corning Research & Development Corporation. A portion of the research was performed using EMSL (grid.436923.9), a DOE Office of Science User Facility sponsored by the Biological and Environmental Research Program. Pacific Northwest National Laboratory is a multi-program national laboratory operated by Battelle for the U.S. DOE under Contract DE-AC05-79RL01830.

Supplementary materials

Supplementary material associated with this article can be found, in the online version, at doi:10.1016/j.scriptamat.2021.114110.

References

[1] W. Holand, G.H. Beall, Glass Ceramic Technology, 2nd Edition, John Wiley & Sons, Inc., Hoboken, New Jersey, 2012.
[2] M.E. McKenzie, B. Deng, D.C. Van Hoesen, X. Xia, D.E. Baker, A. Rezikyan, R.E. Youngman, K.F. Kelton, Sci Rep 11 (1) (2021) 69.
[3] M.E. McKenzie, S. Goyal, T. Loeffler, L. Cai, I. Dutta, D.E. Baker, J.C. Mauro, npj Comput. Mater. 4 (1) (2018).
[4] M.E. McKenzie, J.C. Mauro, Comput. Mater. Sci. 149 (2018) 202–207.
[5] G.H. Beall, D.A. Duke, J. Mater. Sci. 4 (4) (1969) 340–352.
[6] G.H. Beall, L.R. Pinckney, J. Am. Ceram. Soc. 82 (1) (1999) 5–16.
[7] L.R. Pinckney, G.H. Beall, J. Non Cryst. Solids 219 (1997) 219–227.
[8] A.R. Molla, A.M. Rodrigues, S.P. Singh, R.F. Lancelotti, E.D. Zanotto, A.C.M. Rodrigues, M. Reza Dousti, A.S.S. de Camargo, C.J. Magon, I.D.A.A. Silva, J. Am. Ceram. Soc. 100 (5) (2017) 1963–1975.
[9] A.R. Molla, C.R. Kesavulu, R.P.S. Chakradhar, A. Tarafder, S.K. Mohanty, J.L. Rao, B. Karmakar, S.K. Biswas, J. Alloys Compd. 583 (2014) 498–509.
[10] L.R. Pinckney, J. Non Cryst. Solids 255 (2-3) (1999) 171–177.
[11] A.L. Mitchell, C.M. Smith, J. Am. Ceram. Soc. 103 (9) (2020) 4925–4938.
[12] C. Fernandez-Martin, G. Bruno, A. Crochet, D. Ovono Ovono, M. Comte, L. Hennet, W. Lee, J. Am. Ceram. Soc. 95 (4) (2012) 1304–1312.
[13] M. Affatigato, Modern glass characterization, John Wiley & Sons, 2015.
[14] S. Gin, J.V. Ryan, D.K. Schreiber, J. Neeway, M. Cabié, Chem. Geol. 349 (2013) 99–109.
[15] D.E. Perea, D.K. Schreiber, J.V. Ryan, M.G. Wirth, L. Deng, X. Lu, J. Du, J.D. Vienna, npj Mater. Degrad. 4 (1) (2020).
[16] W. Blanc, I. Martin, H. Francois-Saint-Cyr, X. Bidault, S. Chaussedent, C. Hombourger, S. Lacomme, P.Le Coustumer, D.R. Neuville, D.J. Larson, T.J. Prosa, C. Guillermier, J. Phys. Chem. C 123 (47) (2019) 29008–29014.
[17] A. Devaraj, D.E. Perea, J. Liu, L.M. Gordon, T.J. Prosa, P. Parikh, D.R. Diercks, S. Meher, R.P. Kolli, Y.S. Meng, S. Thevuthasan, Int. Mater. Rev. 63 (2) (2017) 68–101.
[18] T.F. Kelly, D.J. Larson, Annu. Rev. Mater. Res. 42 (1) (2012) 1–31.
[19] M.P. Moody, L.T. Stephenson, A.V. Ceguerra, S.P. Ringer, Microsc. Res. Tech. 71 (7) (2008) 542–550.
[20] O.C. Hellman, J.A. Vandenbroucke, J. Rüsing, D. Isheim, D.N. Seidman, Microsc. Microanal. 6 (05) (2002) 437–444.
[21] L. Cormier, O. Dargaud, G. Calas, C. Jousseaume, S. Papin, N. Trcera, A. Cognigni, Mater. Chem. Phys. 152 (2015) 41–47.
[22] O. Dargaud, L. Cormier, N. Menguy, G. Patriarche, J. Non Cryst. Solids 358 (10) (2012) 1257–1262.
[23] O. Dargaud, L. Cormier, N. Menguy, G. Patriarche, G. Calas, Appl. Phys. Lett. 99 (2) (2011).
[24] X. Lu, D.K. Schreiber, J.J. Neeway, J.V. Ryan, J. Du, J. Am. Ceram. Soc. 100 (10) (2017) 4801–4815.
[25] D. Santhanagopalan, D.K. Schreiber, D.E. Perea, R.L. Martens, Y. Janssen, P. Khalifah, Y.S. Meng, Ultramicroscopy 148 (2015) 57–66.
[26] H.S.C. O'Neill, W.A. Dollase, Phys. Chem. Miner. 20 (8) (1994) 541–555.